Atmospheric hydroxyl radical (OH) abundances from ground-based ultraviolet solar spectra: an improved retrieval method

Ross Cheung,[1,*] King Fai Li,[1] Shuhui Wang,[2] Thomas J. Pongetti,[2] Richard P. Cageao,[2] Stanley P. Sander,[2] and Yuk L. Yung[1]

[1]Division of Geological and Planetary Sciences, California Institute of Technology, Pasadena, California 91125, USA

[2]Jet Propulsion Laboratory, California Institute of Technology, Pasadena, California 91109, USA

*Corresponding author: rjc@gps.caltech.edu

The Fourier Transform Ultraviolet Spectrometer (FTUVS) instrument has recorded a long-term data record of the atmospheric column abundance of the hydroxyl radical (OH) using the technique of high resolution solar absorption spectroscopy. We report new efforts in improving the precision of the OH measurements in order to better model the diurnal, seasonal, and interannual variability of odd hydrogen (HO_x) chemistry in the stratosphere, which, in turn, will improve our understanding of ozone chemistry and its long-term changes. Until the present, the retrieval method has used a single strong OH absorption line $P_1(1)$ in the near-ultraviolet at $32,341 \, cm^{-1}$. We describe a new method that uses an average based on spectral fits to multiple lines weighted by line strength and fitting precision. We have also made a number of improvements in the ability to fit a model to the spectral feature, which substantially reduces the scatter in the measurements of OH abundances. © 2008 Optical Society of America

OCIS codes: 010.0010, 010.0280, 300.6300, 300.6540.

1. Introduction

The free radical hydroxyl, OH, plays a key role in atmospheric chemistry from the surface through the mesosphere. Its distribution in the 30–70 km altitude region of the atmosphere is important in determining global stratospheric temperatures and circulation through its influence on the ozone budget [1]. The formation and destruction of ozone in the upper stratosphere and lower mesosphere is controlled mainly by reactions involving odd-hydrogen species ($HO_x = H + OH + HO_2 + 2H_2O_2$), so the understanding of these reactions is crucial to the study of radiative and climatic effects of ozone change [2]. The accuracy of model calculations that describe the coupling between ozone and HO_x radicals has improved significantly in recent years with the availability of satellite data providing vertical profiles of OH and HO_2 throughout the middle and upper atmosphere [3,4].

OH has been measured in the atmosphere by a variety of techniques based on both *in situ* and remote sensing methods. Anderson [5] made the earliest measurement of OH in the upper stratosphere and mesosphere using solar-induced fluorescence in a rocket-borne spectrometer, and Heaps and McGee [6] detected hydroxyl radicals in the stratosphere using balloon-borne LIDAR. There have also been a number of tropospheric and stratospheric balloon-based [7,8], aircraft-based [9–12], and ground-based [11] OH measurements with instruments that use laser-induced fluorescence (LIF) to measure OH and other species. Ground-based *in situ* OH measurements have also been made using chemical ionization mass spectroscopy [13] and long-path UV laser absorption [14]. Several groups have measured rotational lines of OH in the far-infrared, using

balloon and aircraft-borne Fourier transform and Fabry–Perot spectrometers [15–17]. Vertical concentration profiles of OH have also been retrieved from measurements by satellite instruments including the Aura Microwave Limb Sounder (MLS) and Middle Atmosphere High Resolution Spectrograph Investigation (MAHRSI) [3,18,19].

Ground-based solar absorption spectroscopy is an excellent method to address questions related to the variability of upper atmospheric OH on diurnal, seasonal, and interannual time scales, [2]. In this approach, the OH column abundance is retrieved from high resolution UV absorption spectra recorded using the direct solar beam in the $A^2\Sigma^+ \leftarrow X^2\Pi$ (0,0) band near $32,400 \, \text{cm}^{-1}$ (308 nm). This method is selective with respect to OH because there are, in principle, dozens of resolved OH spectroscopic lines that can provide redundant information. However, the strongest of these lines is only a few percent deep, and many other lines suffer interference from solar lines. Nevertheless, the feasibility of this method has been demonstrated by several groups.

OH vertical column measurements have been made at a number of different locations including Fritz Peak Observatory (FPO), Colorado, USA, from 1977 to 2000 [20], Tokyo, Japan, from 1992 to 1995 [21], and Socorro, New Mexico (NMT), USA, from 1996 to 2004 [22,23] using Fabry–Perot and grating spectrographs. From 1998 to the present, OH column abundances have also been measured at the Jet Propulsion Laboratory's Table Mountain Facility (TMF) near Wrightwood, California, USA [24]. The latter measurements employ a Michelson interferometer, the Fourier Transform Ultraviolet Spectrometer (FTUVS), which is described in detail below.

Mills *et al.* [2] have noted that there are systematic differences in the patterns of OH variability and absolute abundance between the Fabry–Perot (FPO, NMT) [21–23] and FTUVS (TMF) [24] results that are not attributable to the geographical differences between the measurement sites. These differences have a significant effect on the comparisons between OH measurements and model calculations regarding effects such as the observed asymmetry between morning and afternoon measurements of the column abundance [25–27], and the absolute magnitude of the summer noontime OH column abundance, which is a factor of 2 smaller in the FTUVS measurements compared with the Fabry–Perot measurements. Since the direct solar OH absorption signal is fairly small, these differences highlight the need to improve the precision of the OH retrievals, which may allow us to discern features in the various cycles of OH that were previously obscured by random noise.

This paper describes a number of the improvements that have been made to the Table Mountain data analysis technique for retrieval of OH column since the publication of Mills *et al.* [2]. These improvements include a systematic procedure to incorporate multiple OH absorption lines into the overall column abundance estimation, a low-pass filter method for removal of baseline effects, and the use of multiple spectral fitting windows. The methods described here are applicable to retrievals of other atmospheric molecules by high resolution spectroscopy.

2. Methods

A. Description of the Table Mountain Fourier Transform Ultraviolet Spectrometer

Since July 1997, the FTUVS has been measuring the OH column abundance over the Table Mountain Facility under sky conditions that range from clear to hazy or partially cloudy. It has a broad spectral coverage, ranging from 4000 to $40,000 \, \text{cm}^{-1}$, and a resolving power over 500,000. This permits an observation of a wide array of atmospheric absorbers including the lines in the $A^2\Sigma^+ \leftarrow X^2\Pi$ (0,0) band of OH. The line strengths at atmospheric average column temperature for the individual rotational lines use absorption cross sections within 0.5% of those used by other groups [20,21]. The OH absorption lines observed by the FTUVS are optically thin, with total column absorption on the order of several percent, so the measurements are sensitive to the entire OH column [2]. The spectroscopy of OH relevant to ground-based column abundance measurements is described in detail in [28].

The FTUVS alternately views the east and west solar limbs of the Sun for 15 minutes on each limb. An average day has about 40 column measurements in the summer and around 25 in the winter. The east and west limb spectra are Doppler shifted relative to one another by the 27-day rotation of the Sun. A spectral shift is applied to the west limb solar spectrum to match the east limb spectrum, the magnitude of which (approximately $0.28 \, \text{cm}^{-1}$) is determined by the minimization of least squares of the residuals of the ratio of the two spectra. The east limb spectrum is then divided by the west limb spectrum, such that the resulting ratio suppresses the solar Fraunhofer features by a factor of 40 or more, leaving mainly the terrestrial OH lines in the spectral window (see Fig. 1). A fit to the Doppler broadened OH lines using a single column temperature (250 K) and cross section for each line results in a slant OH column for each line from the corresponding measured line intensity and absorption cross section. This slant column is divided by the air mass in order to obtain the vertical OH column [24].

The FTUVS instrument operates at ambient pressure but is calibrated relative to the vacuum wavenumber of the helium–neon reference laser. The absolute frequency calibration is therefore subject to an error associated with the difference in the air index of refraction between the UV frequency and the reference laser frequency. This error lies in the range 0.334–$0.338 \, \text{cm}^{-1}$ for the OH spectral features shown in the figures.
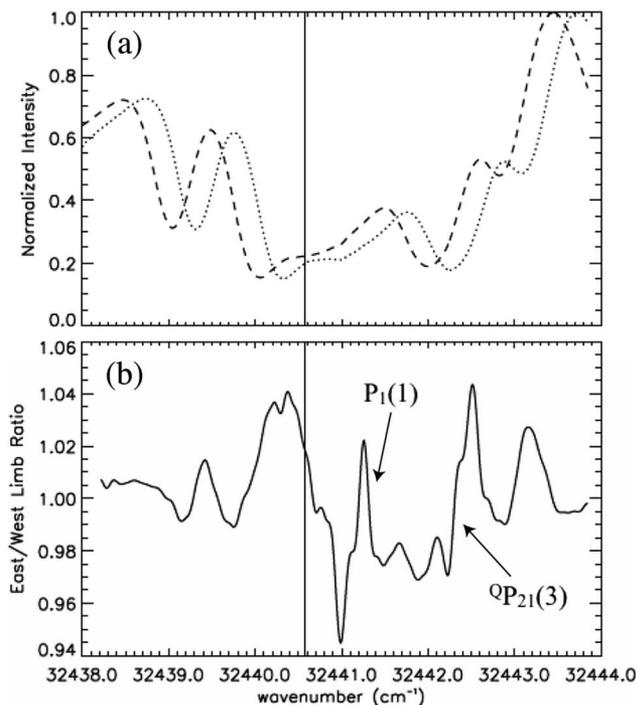
Fig. 1. Ratio of the east and west limb spectra for a spectra close to solar noon on the date 6/13/2005, with the vertical solid line corresponding to the line center for the $P_1(1)$ OH absorption line. The nearby $^QP_{21}(3)$ satellite line is also visible. (a) The TMF instrument alternates between looking at the west limb of the Sun (the dashed line) and the east limb (the dotted line) over the course of the day for 15 minute time steps. (b) The TMF instrument then shifts the west limb over the east limb and takes the ratio of the shifted west limb by the east limb.. The absorption line then stands out prominently while much of the solar background is removed. The frequency difference between the vertical line and the observed OH frequencies is due to a small calibration error (see text).

B. Correction to the Solar Baseline

Following the Doppler solar line suppression procedure described above, the next step is to fit the ratio spectrum to the reference spectrum for each OH absorption line. Especially for the weaker lines, it is important to remove the residual baseline slope. A nonzero baseline slope can be caused by several factors. These include small differences between east and west spectra due to atmospheric turbulence, clouds and aerosols, and the presence of instrument instability leading to phase correction errors. Because of these factors, the linear slope removal technique used in our previous studies (see Fig. 2), which were based on retrievals of the strong $P_1(1)$ and $Q_1(2)$ lines, did not adequately deal with the curved baseline when applied to the weaker lines. With a curved baseline, a linear slope removal often introduced a bias in the retrieved column that can be as large as 10% (Fig. 3).

An alternative approach that significantly increased the retrieval precision involves the application of a fast Fourier transform (FFT) low-pass filter to correct the spectral baseline. The cutoff frequency for the filter was selected such that the narrow OH
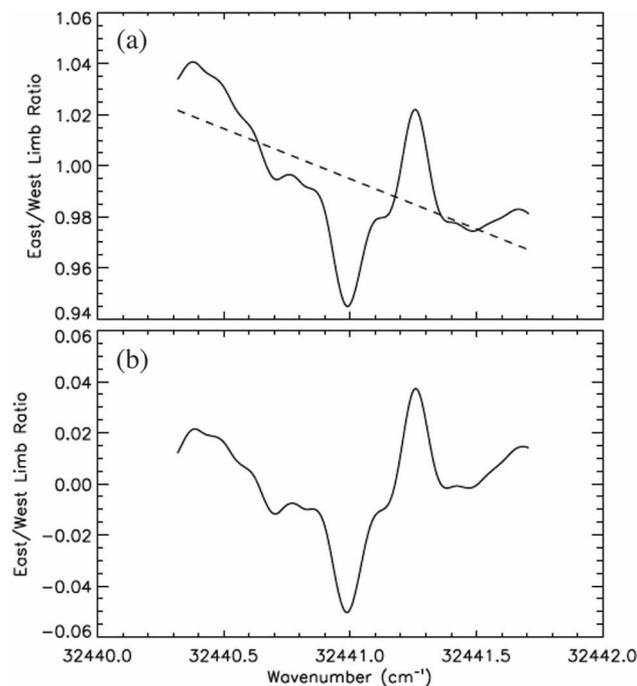

Fig. 2. Linear slope removal technique used in earlier retrieval attempts, applied to the east/west limb ratio spectra in Fig. 1(b). Concerns about artifacts created by a linear slope removal in parts of the solar spectrum with a curved baseline have led to the use of a FFT-low pass filter smoothing method as shown in Fig. 4.

absorption line was not removed in the process. We assumed that the widest OH absorption feature was no wider than $0.5 \, \text{cm}^{-1}$ (the Doppler shift between the east and west limbs, for comparison, was about $0.28 \, \text{cm}^{-1}$) and that, by removing only signals with frequencies lower than $0.5 \, \text{cm}^{-1}$, none of the actual absorption feature would have been removed. Application of a low-pass filter generates a significantly smoother baseline curve, which is then removed from the east/west limb spectra ratio, thus eliminating all of the extraneous solar features before the spectral fit is applied to the OH line (Fig. 4).
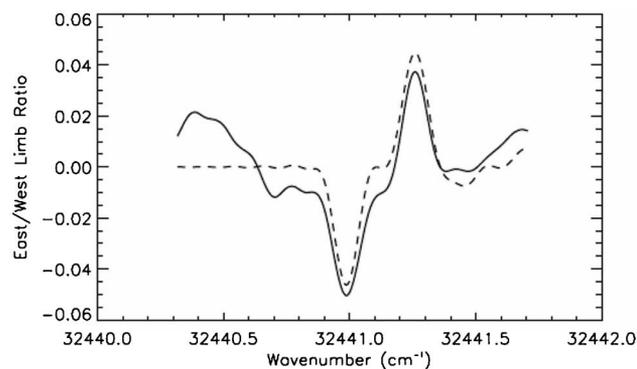

Fig. 3. Doppler model (the dotted line) applied to the ratio of the east and west limbs (the solid line). Higher precision measurements can be obtained by improving this fit, especially in the weaker lines where the Doppler model does not adequately fit the absorption line.
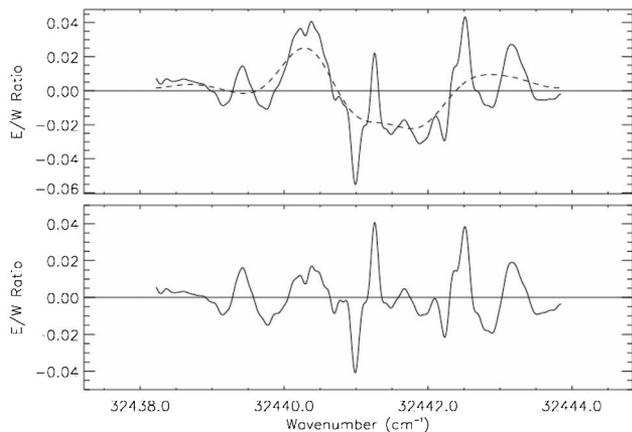
Fig. 4. "Fast-Fourier transform smoothing" method. The dashed line is the baseline obtained by applying a low-pass filter to the entire spectrum, which maps the larger background while ignoring the smaller features such as the absorption lines. The bottom graph shows the spectrum after this baseline is removed.

We have tested a number of techniques in addition to fast Fourier transform filtering, e.g., principal component analysis [29]. It is hard to prove that this is the optimal statistical tool for this analysis. However, we argue that it is adequate for the present purposes.

C. Use of the "Nanowindow" and the Conjugate-Gradient Fit

In the previous analysis, the spectral fit is conducted within a region called the "microwindow" around the absorption line. It was found that much of the background solar variability and noise could be avoided if the Doppler model was applied to a narrow window around the absorption line. We found that care must be taken to select a window narrow enough to eliminate as much of the background noise as possible, which could potentially reduce the precision of the retrieval of the OH column abundance, but not small enough that parts of the absorption feature would be cut off. A final width of four times the full width half-maximum (FWHM) around the peak and valley of each spectral line was used (see Fig. 5), which is slightly wider than the line feature. This reduced window around the line feature, referred to as a "na-
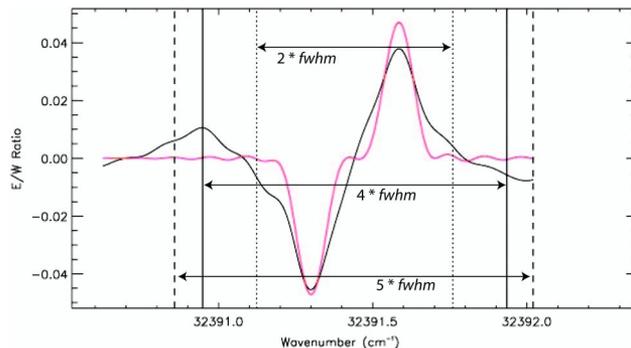

Fig. 5. Sample spectra from the $P_1(2)$ absorption line, which is located in a less optimal region of the solar spectrum. The selection of the right "nanowindow" width can have a pronounced effect on the application of the spectral fit (the red line) to the east/west limb ratio (the black line). A window size too small can cut off part of the absorption signal, resulting in an uneven baseline, and from that a vertical bias in the diurnal OH profile. A window too large introduces additional noise into the retrieval, especially in regions where the solar baseline is especially noisy. We have found that a window width of 4 full widths at half-maximum (fwhm) horizontal from the "peak" and "valley" of the absorption is optimal. The two inner vertical dotted lines show a 2 fwhm window, while the two outer vertical dashed lines show a 5 fwhm window.

nowindow," excludes much of the systematic variability from the solar background.

The conjugate-gradient algorithm was used to obtain the best fit between the spectrum within the nanowindow and the model. The model spectrum includes a second-order polynomial to account for both slope and curvature of the baseline. The coefficients for the polynomial are returned by the conjugate-gradient routine. We found that the second-order term was particularly important for fits to the weaker OH lines, although no significant improvement was found for the stronger lines, such as $P_1(1)$, when the second-order term was included. For the weaker lines, increasing the order of the polynomial to three resulted in no improvement, so a second-order polynomial was used as the standard baseline fitting function.

As shown in Table 1, the new line-fitting approach, which combines the use of a nanowindow with digital filtering to characterize the baseline, and the

Table 1. Five OH Absorption Lines Used in This Analysis[a]

OH Line	Frequency, cm1	Effective Absorption Cross Section, 250 K, 10^{-16} cm^2	Uncertainty of the Mean (Before), %	Uncertainty of the Mean (After), %
$P_1(1)$	32,440.5741	6.787	13	12
$P_1(2)$	32,390.8857	5.660	24	18
$Q_1(2)$	32,458.5918	7.530	15	14
$Q_1(3)$	32,441.8175	5.633	25	21
$P_1(3)$	32,340.5851	3.706	25	23

[a]The frequencies listed are from Stark *et al.* [34]. Also listed is the median 2σ uncertainty of the mean for each line, calculated over the entire dataset from the years 1998–2006, before and after the techniques described in this paper were applied (the histogram of the distribution is shown in Fig. 10). The five lines chosen are the same used in [27], and the calculation of the uncertainty is similar to that described in [30]. One important difference between this calculation and that of [30] is that here the uncertainty is calculated relative to a second order polynomial fit to the diurnal OH profile, rather than relative to a separate linear fit to both the morning and afternoon OH column abundances.

conjugate gradient method to estimate the best-fit parameters, results in significant reductions in the fitting errors. These improvements are in the range of 8–15%, depending on the OH line. Figure 6 shows the effect of the FFT and the "nanowindow" on the vertical bias of the retrieved OH column for several different lines over the course of a typical day. Figure 7 shows a typical spectral fit using the approach described above.

D. Multiple Absorption Line Analysis

The large free spectral range of FTUVS enables the simultaneous observation of multiple OH spectral lines. Within the ~400 cm^{-1} bandpass of the front-end interference filter, over twenty lines in the OH $A^2\Sigma^+\leftarrow X^2\Pi$ (0,0) band have been observed by FTUVS. The groups [20–22] that have employed Fabry–Perot and grating spectrometers to measure OH have all used the $P_1(1)$ line at 32,440.5741 cm^{-1}, because the solar baseline is reasonably flat and the line itself is one of the strongest in the band [30–33].
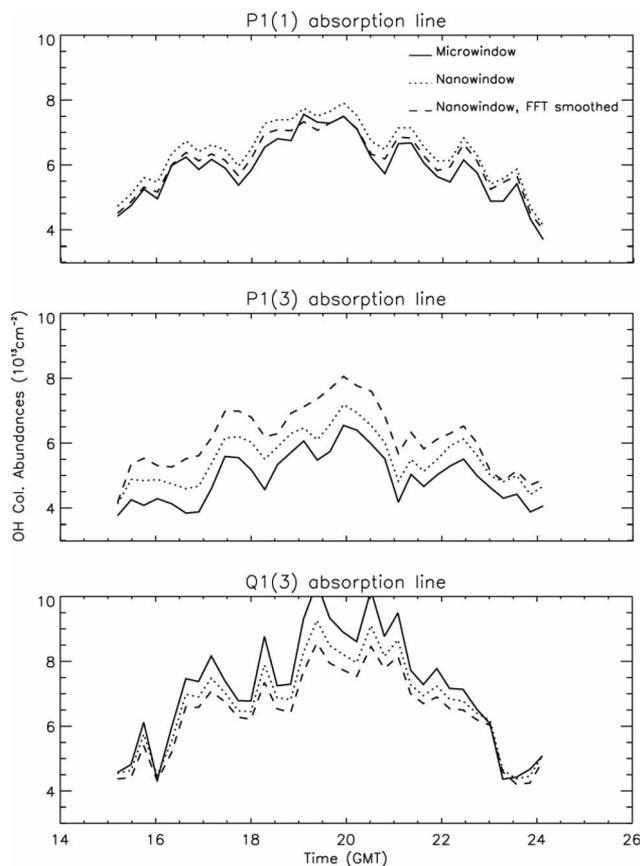

Fig. 6. Comparison of the retrieved diurnal OH column abundances from several different lines over the course of a single day, 5/7/2002. The "microwindow" method uses previous retrieval methods without any of the modifications listed in this paper. The "nanowindow" method uses the nanowindow described in Section 2.C, and the "nanowindow, FFT smoothed" additionally uses the FFT low-pass filter to remove a baseline as described in Section 2.B. Note that we use line-to-line correlation as a good "sanity check" to ensure that the results are accurate, as ideally each line should provide roughly the same column abundances at each time step.
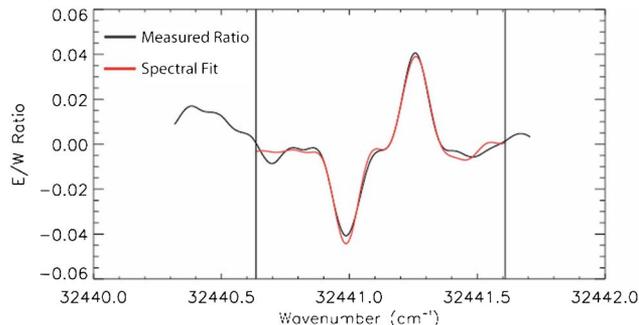

Fig. 7. (Color online) Typical spectral fit showing the measured ratio between the east and the west limbs. The extent of the defined "nanowindow" consists of the area in between the outer two vertical lines, and the spectral fit shows the results of using the conjugate gradient method to improve the fit to the limb spectra within the nanowindow.

An earlier study using TMF spectra also analyzed the $Q_1(2)$ line at 32,458.5918 cm^{-1} [2] with good agreement being observed with the $P_1(1)$ results [30]. The other OH lines are weaker and have greater interference from solar lines, and until recently these have not been reliably retrieved with existing techniques. In a study of the diurnal variability of the OH column from TMF, Li *et al.* incorporated five lines in their retrieval method [27]. This involved fitting a second-order polynomial to the time-dependent OH column abundance from each line and using the average deviation as the weighting factor for averaging multiple lines. This resulted in a substantial reduction in the scatter of the OH diurnal profile compared with data from a single line, but the method introduces the assumption that the profile is second order in time. In addition, this assumption implicitly filters what may be actual temporal anomalies in the OH column. In contrast, the method described here allows the weaker OH lines to be incorporated into the retrieval without the assumptions required by the method of Li *et al.*, As shown in Fig. 6, the "nanowindow" conjugate gradient fit in combination with the FFT filter substantially improves the results derived from the weak $P_1(3)$ and $Q_1(3)$ lines. The correlation between these weak lines and the strong $P_1(1)$ line is sufficiently high to include these and other weak lines in the multiline analysis.

For the five strongest and most reliable lines, we have carried out multiple-line analyses consisting of a weighted average of the column abundances from each of the five lines in Table 1, which are the same five lines used by Li *et al.* [27]. These five lines were chosen from among the twenty strongest OH absorption lines in the $A^2\Sigma^+\leftarrow X^2\Pi$ (0,0) band. The criteria for selection involved determining the respective spectral fit uncertainty for each line over a large data set, with the measurement error defined by the variance between the spectral fit and the actual measurement. From a close inspection of the spectral fit uncertainty, the five OH absorption lines listed in Table 1 were chosen for the present analysis.

While the five lines selected for the retrieval provide independent information on the OH column abundance, they are not of uniform quality primarily because of differences in the slopes of the underlying Fraunhofer features, and because some lines are weaker than others. The Doppler differencing method does not suppress the solar features completely, and remnants of these features contribute a systematic offset to the line fitting results, particularly for the weaker lines. Ordinarily, the OH column abundance would be derived from a weighted average of the results from the five OH lines, where the weighting factors are derived from the inverse of the variance of the fit to each line. Because the residual solar features can introduce a bias, we have adopted a different weighting scheme that provides a better measure of the data quality and that makes no assumptions concerning the shape of the diurnal OH column profile as in Li *et al.* [27]. The OH columns derived from the five spectral lines were averaged with weighting factors derived from the signal-to-noise ratio, defined as the peak to valley amplitude of the absorption line divided by the variance, or the ordinary least squares of the spectral fit residuals, as a weighting factor (see Figs. 8 and 9). This was found to be the best weighting method as it takes into account the relative strength of the line (from the amplitude) and the spectral fit uncertainty (from the variance). In addition, because the quality of the spectral fit varied over the course of a day, this method provided a specific, yet meaningful, weighting system for each time step, while the parabolic fitting method of Li *et al.* averaged over an entire day.

One additional step in the OH retrieval is the use of "dynamic line selection." Starting with the fit to the strongest line, $P_1(1)$, the OH column derived from the fit to each of the other lines is consecutively added to the weighted sum, and after each addition the least squares deviation of the diurnal weighted average from a second order polynomial fit is calculated. If the deviation increased with the addition of
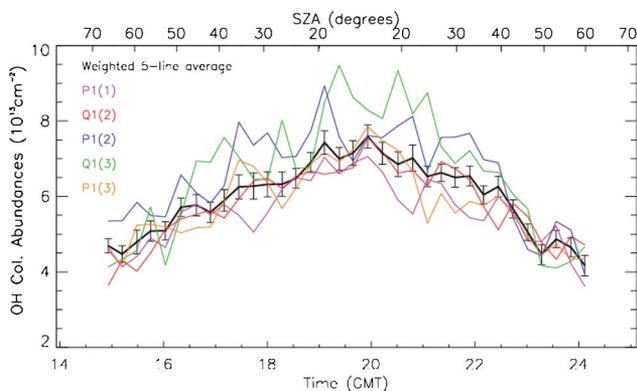

Fig. 8. (Color online) Graph of the diurnal OH abundances by solar hour angle for a sample day, 5/7/2002. Note that the black line is the weighted average of all of the five individual lines weighted by their signal-to-noise ratio. The error bars correspond to the calculated 1-standard deviation for the five-line weighted average calculated OH column abundance.
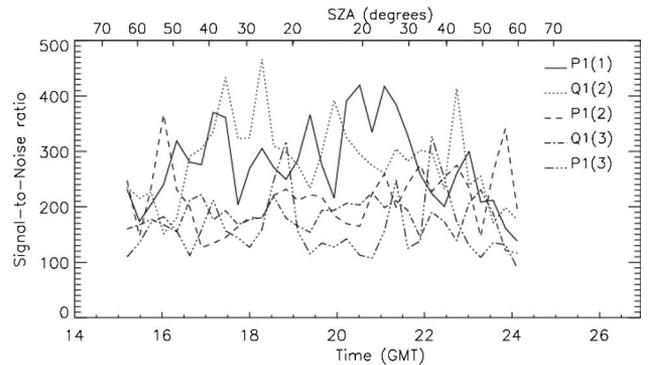

Fig. 9. "Signal-to-noise" ratios as defined in Section 2.D over the course of a sample day, 5/7/2002. A higher signal-to-noise ratio means that the corresponding column abundance for that line received a larger weighting for the multiple-line average for that one specific time.

the line, then the entire diurnal OH profile retrieved from that line would be rejected from the final weighted average. If the deviation decreased, then we assumed that the line contained meaningful data, and the line would be included in the final weighting.

OH lines other than those listed in Table 1 rarely passed the test for inclusion in the weighted sum, using the dynamic line selection criterion. We therefore conclude that these five lines contribute the most to the overall retrieval precision, with additional lines providing no useful information.

3. Results

The inclusion of the FFT filtering step, the use of the conjugate gradient fit, and the use of the "signal-to-noise ratio" of each spectral fit instead of the variance of the diurnal OH column profile as a weighting factor have resulted in significant improvements in the measurement and retrieval of OH abundances compared with our previous algorithm. It was found while using dynamic selection that, although the results varied greatly from day to day, for cloud-free days in the summer all five lines met the criterion for inclusion in the weighted average, while for many winter and partially cloudy days, only two or three lines met the criterion.

A few data sets, mainly from the first two years of operation of the FTUVS instrument (1998–1999), have particularly high noise levels. The resulting column retrievals disagree with the average OH abundance for the corresponding season and time of day from subsequent years. These outliers were only seen from the beginning of 1998 until the spring of 2000 after which the OH retrievals show much higher precision. A careful inspection of the outliers revealed that the weaker OH absorption lines, primarily $P_1(3)$, but occasionally $P_1(2)$ or $Q_1(3)$, were not yielding any OH column results; in effect, they lacked an absorption line shape, and the retrieval method was attempting to fit background noise, resulting in extremely erratic OH column measurements over the course of the day. The improvements in the quality of the data around the weaker lines resulted from
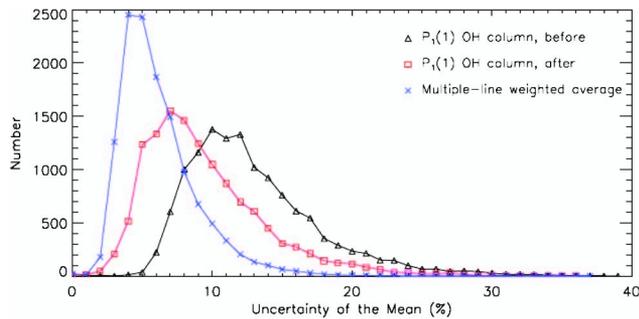
Fig. 10. Comparison of the histograms of the 2σ OH column uncertainty of the mean (Δ column/column) for the $P_1(1)$ OH line over TMF from 1998–2006 with and without the methods described in this paper, and for the dynamically selected five-line weighted average. The method here is similar to that used to find Fig. 2 of Mills *et al.* [30], except that the deviation is calculated from a second order polynomial fit to the diurnal OH column abundances, instead of two separate linear fits to the morning and afternoon OH abundances.

upgrades to the FTUVS instrument, which included the use of a more sensitive detector (silicon avalanche photodiode) and recoating and alignment of the telescope optics to improve the throughput. The dynamic line selection method corrects the instrumental artifact that would otherwise cause significant errors when taking a multiple-weighted line average in data from the years before the spring of 2000.

Table 1 shows the changes in the median spectral fit uncertainty of the five OH absorption lines used in this analysis. In general, there were some improvements in the stronger OH absorption lines, $P_1(1)$ and $Q_1(2)$, but the most dramatic reductions in spectral fit error occurred in some of the weaker absorption lines or in the lines in noisier regions of the spectrum. Figure 10 shows the histogram of the 2σ uncertainty of the $P_1(1)$ absorption line fits with and without the improved fitting techniques described here, as well as the uncertainty of the dynamically selected multiple-line weighted average, which was in general lower than uncertainty from any of the individual lines. Note that $P_1(1)$ was the absorption line that generally produced the best results. The improvement in the fitting precision for the weaker lines was usually larger than that observed for the $P_1(1)$ line.

4. Summary and Conclusions

Since 1998, the Jet Propulsion Laboratory's Table Mountain Facility has been observing column OH abundances daily from solar zenith angles of 10° to 80°, using a ground-based Fourier transform ultraviolet spectrometer (FTUVS). In the present work, an improved scheme for the retrieval of OH column abundances is described. The new features of this scheme include (1) FFT low-pass filtering for improved correction of the spectral baseline, (2) use of the conjugate gradient method to fit the OH line shape within a "nanowindow" nested within the spectral microwindow, and (3) averaging of multiple OH absorption lines weighted by the line strength and quality of the spectral fits for each line. These improvements have increased the precision of the OH retrievals by 10–20%, increasing the utility of the FTUVS OH data for the analysis of short-term variability (such as the AM/PM diurnal asymmetry), long-term trends (for example, the 11-year solar cycle), and satellite validation.

References

1. R. Müller, and R. J. Salawitch, "Upper stratospheric processes," in *Scientific Assessment of Ozone Depletion: 1998*, D. L. Albritton, ed. (World Meteorological Organization, 1999), pp. 6.1–6.44.

2. F. P. Mills, R. P. Cageao, S. P. Sander, M. Allen, Y. L. Yung, E. E. Remsberg, J. M. Russell III, and U. Richter, "OH column abundance over Table Mountain Facility, California: intra-annual variations and comparisons to model predictions for 1997–2001," J. Geophys. Res. **108** 4785 (2003).

3. S. Wang, H. M. Pickett, T. J. Pongetti, R. Cheung, Y. L. Yung, C. Shim, Q. Li, T. Canty, R. J. Salawitch, K. W. Jucks, B. Drouin, and S. P. Sander, "Validation of aura MLS OH measurement with FTUVS total OH column measurement at TMF, California," J. Geophys. Res. (to be published).

4. H. M. Pickett and D. B. Peterson, "Comparison of measured stratospheric OH with prediction," J. Geophys. Res. **101**, 16789–16796 (1996).

5. J. G. Anderson, "Rocket measurement of OH in the mesosphere," J. Geophys. Res. **76**, 7820–7824 (1971).

6. W. S. Heaps and T. J. McGee, "Progress in stratospheric hydroxyl measurement by balloon-borne LIDAR," J. Geophys. Res. **90**, 7913–7921 (1985).

7. R. M. Stimpfle and J. G. Anderson, "In situ detection of OH in the lower stratosphere with a balloon borne high repetition rate laser system," Geophys. Res. Lett. **15**, 1503–1506 (1988).

8. R. M. Stimpfle, P. O. Wennberg, L. B. Lapson, and J. G. Anderson, "Simultaneous, in situ measurements of OH and HO$_2$ in the stratosphere," Geophys. Res. Lett. **17**, 1905–1908 (1990).

9. P. O. Wennberg, R. C. Cohen, N. L. Hazen, L. B. Lapson, N. T. Allen, T. F. Hanisco, J. F. Oliver, N. W. Lanham, J. N. Demusz, and J. G. Anderson, "Aircraft-borne, laser-induced fluorescence instrument for the in situ detection of hydroxyl and hydroperoxyl radicals," Rev. Sci. Instrum. **65**, 1858–76 (1994).

10. P. O. Wennberg, T. F. Hanisco, R. C. Cohen, R. M. Stimpfle, L. B. Lapson, and J. G. Anderson, "In situ measurements of OH and HO$_2$ in the upper troposphere and stratosphere," J. Atmos. Sci. **19**, 3412–3420 (1995).

11. I. C. Faloona, D. Tan, R. L. Lesher, N. L. Hazen, C. L. Frame, J. B. Simpas, H. Harder, M. Martinez, P. Di Carlo, X. Ren, and W. H. Brune, "Laser-induced fluorescence instrument for detecting tropospheric OH and HO$_2$: characteristics and calibration," J. Atmos. Chem. **47**, 139–167 (2004).

12. W. J. Bloss, T. J. Gravestock, D. E. Heard, T. Ingham, G. P. Johnson, and J. D. Lee, "Application of a compact all solid-state laser system to the in situ detection of atmospheric OH, HO$_2$, NO, and IO by laser-induced fluorescence," J. Environ. Monitor. **5**, 21–28 (2003).

13. H. Berresheim, T. Elste, C. Plass-Dulmer, F. L. Eisele, and D. J. Tanner, "Chemical ionization mass spectrometer for long-term measurement of atmospheric OH and HO$_2$SO$_4$," Int. J. Mass Spectrom. **202**(1–3), 91–109 (2000).

14. G. H. Mount, "The measurement of tropospheric OH by long path absorption 1. Instrumentation," J. Geophys. Res. **97**, 2427 (1992).

15. J. H. Park and B. Carli, "Spectroscopic measurement of HO$_2$, H$_2$O$_2$, and OH in the stratosphere," J. Geophys. Res. **96**, 22535–22541 (1991).

16. D. G. Johnson, K. W. Jucks, W. A. Traub, and K. V. Chance, "Smithsonian stratospheric far-infrared spectrometer and data reduction system," J. Geophys. Res **100**, 3091–3106 (1995).

17. H. M. Pickett and D. B. Peterson, "Stratospheric OH measurements with a far-infrared limb observing spectrometer," J. Geophys. Res. Atmos. **98**, 20507–20515 (1993).

18. R. R. Conway, M. H. Stevens, J. G. Cardon, S. E. Zasadil, C. M. Brown, J. S. Morrill, and G. H. Mount, "Satellite measurements of hydroxyl in the mesosphere," Geophys. Res. Lett. **23**, 2093–2096 (1996).

19. R. R. Conway, M. H. Stevens, C. M. Brown, J. G. Cardon, S. E. Zasadil, and G. H. Mount, "Middle Atmosphere High Resolution Spectrograph Investigation," J. Geophys. Res. **104**, 16327–16348 (1999).

20. C. R. Burnett and E. B. Burnett, "The regime of decreased OH vertical column abundances at Fritz Peak Observatory, CO: 1991–1995," Geophys. Res. Lett. **23**, 1925–1927 (1996).

21. N. Iwagami, S. Inomata, and T. Ogawa, "Doppler detection of hydroxyl column abundance in the middle atmosphere: 2. Measurement for three years and comparison with a 1D model," J. Atmos. Chem. **29**, 195–216 (1998).

22. C. R. Burnett and K. Minschwaner, "Continuing development in the regime of decreased atmospheric column OH at Fritz Peak, Colorado," Geophys. Res. Lett. **25**, 1313–1316 (1998).

23. T. Canty, K. Minschwaner, K. W. Jucks, and A. K. Smith, "A review of hydroxyl in the middle atmosphere: comparison of measured and modeled vertical profiles and ground-based column observations," in Vol. 123 of *Atmospheric Sciences Across the Stratopause, Geophysical Monograph Series*, E. Siskind, S. D. Eckermann, and M. E. Summers, eds. (American Geophysical Union, 2000), pp. 131–136.

24. R. P. Cageao, J. F. Blavier, J. P. McGuire, Y. Jiang, V. Nemtchinov, F. P. Mills, and S. P. Sander, "High-resolution Fourier-transform ultraviolet-visible spectrometer for the measurement of atmospheric trace species: application to OH," Appl. Opt. **40**, 2024–2030 (2001).

25. C. R. Burnett, K. R. Minschwaner, and E. B. Burnett, "Vertical column abundance measurements of atmospheric hydroxyl from 26°N, 40°N, and 65°N," J. Geophys. Res. **93**, 5241–5253 (1988).

26. M. J. Prather, "Ozone in the upper stratosphere and mesosphere," J. Geophys. Res. **86**, 5325–5338 (1981).

27. K. F. Li, R. P. Cageao, E. M. Karpilovsky, F. P. Mills, Y. L. Yung, J. S. Margolis, and S. P. Sander, "OH column abundance over Table Mountain Facility, California: AM-PM diurnal asymmetry," Geophys. Res. Lett. **32**, L13813 (2005).

28. R. P. Cageao, Y. L. Ha., Y. Jiang, M. F. Morgan, Y. L. Yung, and S. P. Sander, "Calculated hydroxyl $A^2\Sigma \to X^2\Pi$ $(0,0)$ band emission rate factors applicable to atmospheric spectroscopy," J. Quant. Spectrosc. Radiat. Transfer **57**, 703–717 (1997).

29. R. W. Preisendorfer, *Principal Component Analysis in Meteorology and Oceanography* (Elsevier Science, 1988), p. 425.

30. F. P. Mills, R. P. Cageao, V. Nemtchinov, Y. Jiang, and S. P. Sander, "OH column abundance over Table Mountain Facility, California: annual average 1997–2000," Geophys. Res. Lett. **29**, 1742 (2002),

31. N. Iwagami, S. Inomata, I. Murata, and T. Ogawa, "Doppler detection of hydroxyl column abundance in the middle atmosphere," J. Atmos. Chem. **20**, 1–15 (1995).

32. J. Notholt, H. Schutt, and A. Keens, "Solar absorption measurements of stratospheric OH in the UV with a Fourier-transform spectrometer," Appl. Opt. **36**, 6076–6082 (1997).

33. C. R. Burnett and E. B. Burnett, "Spectroscopic measurements of the vertical column abundance of hydroxyl (OH) in the earth's atmosphere," J. Geophys. Res. **86**, 5185–5202 (1981).

34. G. Stark, J. W. Brault, M. C. Abrams, "Fourier-transform spectra of the A$A^2\Sigma^+ \to X^2\Pi$ $\Delta v = 0$ bands of OH and OD," J. Opt. Soc. Am. B **11**, 3–32 (1994).